

Rotational fluctuation of molecules in quantum clusters. I. Path integral hybrid Monte Carlo algorithm

メタデータ	言語: eng 出版者: 公開日: 2017-10-03 キーワード (Ja): キーワード (En): 作成者: メールアドレス: 所属:
URL	https://doi.org/10.24517/00010276

This work is licensed under a Creative Commons Attribution-NonCommercial-ShareAlike 3.0 International License.



Rotational fluctuation of molecules in quantum clusters. I. Path integral hybrid Monte Carlo algorithm

Shinichi Miura^{a)}*Institute for Molecular Science, 38 Myodaiji, Okazaki 444-8585, Japan*

(Received 15 December 2006; accepted 9 February 2007; published online 20 March 2007)

In this paper, we present a path integral hybrid Monte Carlo (PIHMC) method for rotating molecules in quantum fluids. This is an extension of our PIHMC for correlated Bose fluids [S. Miura and J. Tanaka, *J. Chem. Phys.* **120**, 2160 (2004)] to handle the molecular rotation quantum mechanically. A novel technique referred to be an effective potential of quantum rotation is introduced to incorporate the rotational degree of freedom in the path integral molecular dynamics or hybrid Monte Carlo algorithm. For a permutation move to satisfy Bose statistics, we devise a multilevel Metropolis method combined with a configurational-bias technique for efficiently sampling the permutation and the associated atomic coordinates. Then, we have applied the PIHMC to a helium-4 cluster doped with a carbonyl sulfide molecule. The effects of the quantum rotation on the solvation structure and energetics were examined. Translational and rotational fluctuations of the dopant in the superfluid cluster were also analyzed. © 2007 American Institute of Physics.
[DOI: 10.1063/1.2713395]

I. INTRODUCTION

Chemical processes in helium nanodroplets have been revealed to exhibit exotic properties due to quantum fluctuations of the medium.¹⁻⁴ Unlike in the usual condensed environments, for example, molecules dissolved in the ultracold nanodroplet of ⁴He atoms are found to rotate freely in an effective manner.⁵ This behavior arises from the superfluidity of the nanodroplet. Conversely, the nanodroplets can be regarded as an ideal matrix for performing the spectroscopic measurements, since the helium nanodroplets are characterized by extremely low temperatures and the superfluidity.^{1,2} While the spectroscopic measurements have been carried out using the nanodroplets consisting of several thousand atoms, recent experimental advances allow the study of clusters containing one to about 20 helium-4 atoms, showing the size dependence on the molecular motion doped in the clusters.⁶⁻¹⁰ Very recent spectroscopic study on the doped helium clusters reveals rich size dependence of the dopant rotational fluctuation in the size up to $N=72$.¹¹ In this paper (paper I) and a companion paper (paper II),¹² molecular fluctuations of the dopants in the helium-4 cluster are studied in detail using a path integral simulation technique. In the paper I, we present a path integral hybrid Monte Carlo method for rotating molecules in quantum fluids. In the paper II, cluster-size dependence on the rotational fluctuation of a carbonyl sulfide (OCS) molecule is analyzed, being connected with the onset of the superfluidity of the helium-4 clusters.

Microscopic fluctuations in the helium-4 clusters at finite temperatures have theoretically been studied by quantum simulation techniques.¹³ The pure helium-4 clusters were

first studied by the path integral Monte Carlo (PIMC) method, which predicted that the superfluidity can be observed even in a finite system such as clusters.¹⁴ Then, the structural fluctuations of the doped helium-4 clusters were examined by the PIMC calculations where the dopant molecule was approximated as a classical object fixed at the origin.^{3,15-18} The solvation structure of the dopant in the superfluid helium-4 cluster was characterized via the long exchange cycles of the helium paths arising from the Bose statistics. Although the effect of the rotational fluctuation of the heavy dopant had been expected to be small on the structure, the significant effect was found even in the density profile of the helium-4 around the molecule using the ground-state quantum Monte Carlo (QMC) method.¹⁹ Also, the rotational fluctuation of the dopant in superfluid, which is dramatically influenced by the quantum fluctuation of the medium, cannot directly be accessed since the molecule is fixed in space. Then, the molecular rotation in the helium-4 clusters at the ground-state was studied by the QMC techniques.²⁰⁻²⁴ For finite temperature calculations corresponding to the experimental condition, we developed a path integral hybrid Monte Carlo (PIHMC) method to handle the molecular rotation quantum mechanically, and reported preliminary results on the OCS molecule in a helium-4 cluster.²⁵ Independently, Zillich *et al.*²⁶ and Blinov and Roy²⁷ extended the PIMC technique to rotating molecules in superfluids. In this paper, we present the full account on our PIHMC method for rotors in superfluids.

The path integral hybrid Monte Carlo method for rotating molecules in superfluids consists of two types of trial moves, since the system to be sampled is characterized by two types of variables; one is the path variables describing translational and rotational fluctuations of the system, and the other is the permutation needed to satisfy the Bose statistics. In the PIHMC method, the path variables are sampled

^{a)}Permanent address: Division of Mathematical and Physical Sciences, Graduate School of Natural Science and Technology, Kanazawa University, Kakuma, Kanazawa 920-1192, Japan. Electronic mail: miura@cphys.s.kanazawa-u.ac.jp

by the so-called hybrid Monte Carlo (HMC).^{28–30} Unlike the standard Metropolis method, the HMC simultaneously moves the whole systems coordinates on the basis of equations of motion. The trial configuration generated by the molecular dynamics is accepted or rejected by a suitable Metropolis criterion. In the present study, a novel technique to incorporate the quantum rotational motion, which is referred to be an effective potential of quantum rotation, is presented to construct a path integral molecular dynamics or hybrid Monte Carlo for rigid bodies. On the other hand, the permutation and the associated path variables are sampled by a multilevel Metropolis method developed by Ceperley.¹³ In order to enhance the sampling efficiencies, we apply an idea of a configurational-bias Monte Carlo³¹ to the multilevel Metropolis method.

This paper is organized as follows. The methodology is described in Sec. II. Computational details are given in Sec. III. Calculated results on a doped helium-4 cluster OCS(⁴He)₆₄ are presented in Sec. IV. Methodological aspects are discussed in Sec. V.

II. METHODOLOGY

A. The partition function

We consider a system consisting of a linear molecule and N helium-4 atoms; the molecule is modeled as a rigid rotor. The OCS molecule is chosen as a dopant in the present study. The system is described by the following Hamiltonian:

$$H = \sum_{i=1}^{N+1} \frac{\mathbf{p}_i^2}{2m_i} + \frac{\mathbf{L}^2}{2I_{\text{OCS}}} + V_{\text{He-He}} + V_{\text{He-OCS}}. \quad (1)$$

The first term in Eq. (1) is the translational kinetic energy represented by the linear momentum of the i th particle \mathbf{p}_i with the associated mass m_i . Here, the last particle labeled as $N+1$ is assigned to the center of mass of the OCS molecule. The second term is the rotational kinetic energy by the angular momentum of the OCS molecule \mathbf{L} with the moment of inertia I_{OCS} . The helium-helium interaction $V_{\text{He-He}}$ is represented by the sum of a pair interaction, and the helium-OCS interaction is written as

$$V_{\text{He-OCS}} = \sum_{i=1}^N v_{\text{He-OCS}}(\mathbf{r}_i - \mathbf{r}_{N+1}, \Omega), \quad (2)$$

where \mathbf{r}_i is the position of the i th particle and Ω represents the orientation of the molecule in the laboratory frame.

In order to obtain a discretized path integral expression of the partition function, we first write the partition function at an inverse temperature $\beta = 1/k_B T$ as the product of a high temperature density matrix $\rho(\Delta\tau)$ at $\Delta\tau = \beta/M$ in the coordinate space by^{13,32}

$$Z = \frac{1}{N!} \sum_{\mathcal{P}} \int \cdots \int \left\{ \prod_{s=1}^M d\mathbf{R}^{(s)} d\Omega^{(s)} \right\} \times \prod_{s=1}^M \rho(\mathbf{R}^{(s)}, \Omega^{(s)}, \mathbf{R}^{(s+1)}, \Omega^{(s+1)}; \Delta\tau), \quad (3)$$

where \mathbf{R} denotes collectively the atomic positions including

the center of mass of the molecule: $\mathbf{R} = (\mathbf{r}_1, \dots, \mathbf{r}_{N+1})$; the superscript s labels the imaginary time slice. The summation in Eq. (3) is taken over all possible permutation \mathcal{P} to account for the indistinguishability of the helium-4 atoms. In the present study, the high temperature density matrix is approximated by

$$\rho(\mathbf{R}, \Omega, \mathbf{R}', \Omega'; \Delta\tau) \simeq \rho^{\text{tra}}(\mathbf{R}, \mathbf{R}'; \Delta\tau) \rho^{\text{rot}}(\Omega, \Omega'; \Delta\tau) \rho^{\text{int}}(\mathbf{R}, \Omega, \mathbf{R}', \Omega'; \Delta\tau). \quad (4)$$

Here, $\rho^{\text{tra}}(\mathbf{R}, \mathbf{R}'; \Delta\tau)$ and $\rho^{\text{rot}}(\Omega, \Omega'; \Delta\tau)$, respectively, denote the density matrices of the free translation and rotation at the inverse temperature $\Delta\tau$, and $\rho^{\text{int}}(\mathbf{R}, \Omega, \mathbf{R}', \Omega'; \Delta\tau)$ represents the interacting part of the density matrix. The translational density matrix is written by^{33,34}

$$\rho^{\text{tra}}(\mathbf{R}, \mathbf{R}'; \Delta\tau) = \prod_{i=1}^{N+1} \left(\frac{m_i}{2\pi\Delta\tau\hbar^2} \right)^{3/2} e^{-\sum_{i=1}^{N+1} (m_i/2\Delta\tau\hbar^2)(\mathbf{r}_i - \mathbf{r}'_i)^2} \quad (5)$$

and the rotational density matrix by³²

$$\rho^{\text{rot}}(\Omega, \Omega'; \Delta\tau) = \sum_{J=0}^{\infty} \frac{2J+1}{4\pi} e^{-\Delta\tau B_{\text{OCS}} J(J+1)} P_J(\mathbf{e} \cdot \mathbf{e}'), \quad (6)$$

where the rotational constant $B_{\text{OCS}} = \hbar^2/2I_{\text{OCS}}$ and P_J is a Legendre polynomial. The unit vector \mathbf{e} represents the molecular axis of the OCS with respect to the laboratory frame. Unlike the translational density matrix, the rotational density matrix cannot be simplified further analytically. Thus, we define a potential function u^{rot} using the above rotational density matrix: $e^{-\Delta\tau u^{\text{rot}}(\Omega, \Omega')} \equiv \rho^{\text{rot}}(\Omega, \Omega'; \Delta\tau)$. We refer to it as an effective potential of quantum rotation. Here, we consider the high temperature limit of the effective potential. At enough high temperature, the effective potential can be expressed by

$$\Delta\tau u^{\text{rot}}(\Omega, \Omega') = \frac{\beta}{2} I_{\text{OCS}} \omega_M^2 \gamma^2 + \text{const}, \quad (7)$$

since the rotational density matrix at the high temperature can be written by $\rho^{\text{rot}}(\Omega, \Omega') \propto e^{-(1/4B_{\text{OCS}}\Delta\tau)\gamma^2}$ where $\cos\gamma = \mathbf{e} \cdot \mathbf{e}'$.³⁵ Thus, the effective potential essentially works as a “restoring force” with a characteristic frequency $\omega_M = \sqrt{M/\beta\hbar}$ regarding the angle γ for linear rotors.

Regarding the interacting part of the density matrix, ρ^{int} is written based on a hybrid use of a pair density matrix approximation^{13,36} for the He-He correlation and an expression exact up to $\mathcal{O}((\Delta\tau)^4)$ by Marx and Muser³² and Takahashi and Imada³⁷ for the He-OCS correlation as

$$\rho^{\text{int}}(\mathbf{R}, \Omega, \mathbf{R}', \Omega'; \Delta\tau) = e^{-\Delta\tau\{U_{\text{He-He}}(\mathbf{R}, \mathbf{R}') + V_{\text{He-OCS}}(\mathbf{R}, \Omega) + V_{\text{corr}}(\mathbf{R}, \Omega)\}}, \quad (8)$$

where $U_{\text{He-He}}$ is written by the sum of an effective interaction defined via the exact pair density matrix.^{38,39} The higher order correction term V_{corr} can be written by^{32,37}

$$V_{\text{corr}} = \frac{(\Delta\tau)^2}{24} \left\{ \sum_{i=1}^{N+1} \frac{\hbar^2}{m_i} \left(\frac{\partial V_{\text{He-OCS}}}{\partial \mathbf{r}_i} \right)^2 + \frac{\hbar^2}{I_{\text{OCS}}} \left\{ \left(\frac{\partial V_{\text{He-OCS}}}{\partial \mathbf{e}} \right)^2 - \left(\mathbf{e} \cdot \frac{\partial V_{\text{He-OCS}}}{\partial \mathbf{e}} \right)^2 \right\} \right\}. \quad (9)$$

When we neglect the correction term V_{corr} , Eq. (8) becomes the hybrid expression of the pair density matrix and the primitive approximations which has been used in PIMC calculations of the fixed OCS molecule dissolved in the helium-4 clusters.^{3,17} Using the above expressions, the partition function in the discretized path integral can be summarized as

$$Z = \frac{1}{N!} \sum_{\mathcal{P}} \prod_{i=1}^{N+1} \left(\frac{m_i M}{2\pi\beta\hbar^2} \right)^{3M/2} \int \cdots \int \left\{ \prod_{s=1}^M d\mathbf{R}^{(s)} d\Omega^{(s)} \right\} \times e^{-S(\{\mathbf{R}\}, \{\Omega\}, \mathcal{P})}, \quad (10)$$

where the imaginary time action $S(\{\mathbf{R}\}, \{\Omega\}, \mathcal{P})$ is written by

$$S = \sum_{s=1}^M \sum_{i=1}^{N+1} \frac{m_i M}{2\beta\hbar^2} (\mathbf{r}_i^{(s)} - \mathbf{r}_i^{(s+1)})^2 + \Delta\tau \sum_{s=1}^M u^{\text{rot}}(\Omega^{(s)}, \Omega^{(s+1)}) + \Delta\tau \sum_{s=1}^M \{ U_{\text{He-He}}(\mathbf{R}^{(s)}, \mathbf{R}^{(s+1)}) + V_{\text{He-OCS}}(\mathbf{R}^{(s)}, \Omega^{(s)}) + V_{\text{corr}}(\mathbf{R}^{(s)}, \Omega^{(s)}) \}. \quad (11)$$

Here, $\{\mathbf{R}\}$ denotes the coordinates collectively over all time slices: $\{\mathbf{R}\} = (\mathbf{R}^{(1)}, \dots, \mathbf{R}^{(M)})$, and $\{\Omega\}$ is defined similarly. Then, sampling method is constructed so as to generate configurations of the system proportional to the following weight π :

$$\pi(\{\mathbf{R}\}, \{\Omega\}, \mathcal{P}) \propto e^{-S(\{\mathbf{R}\}, \{\Omega\}, \mathcal{P})}. \quad (12)$$

In the present study, the path variables $\{\mathbf{R}\}$ and $\{\Omega\}$ and the permutation \mathcal{P} are sampled using two types of trial moves. The path variables are sampled by the HMC move based on a path integral molecular dynamics method, and the permutation by the multilevel Metropolis method combined with the configurational-bias Monte Carlo technique. To guarantee the symmetry of the underlying Markov chain, the selection

of the type of move (HMC or permutation) should be probabilistic rather than deterministic in the course of the simulation.³¹ In the following two subsections, these methods are described separately.

B. Path-variable sampling

The hybrid Monte Carlo²⁸⁻³⁰ is a method that combines molecular dynamics (MD) and Monte Carlo (MC) techniques. Unlike the conventional MC, whole system coordinates are simultaneously updated by equations of motion. The trial configuration is then accepted by an appropriate Metropolis criterion as in MC. The HMC algorithm has been proven to yield the canonical distribution as long as a time-reversible and area-preserving numerical integration algorithm is employed to solve the equations of motion; this condition is needed so as to guarantee the microscopic detailed balance.²⁹ In the present study, the HMC method is used to sample the path variables $\{\mathbf{R}\}$ and $\{\Omega\}$ with the permutation \mathcal{P} fixed. In the following, appropriate equations of motion are described.

First, we define an effective potential function W_{eff} using the imaginary time action: $W_{\text{eff}} = S/\beta$. Then, the partition function can be regarded as the configurational integral of a polymeric system at the inverse temperature β characterized by W_{eff} .^{40,41} As in our previous study,³⁹ we adopt the staging variable $\mathbf{u}_i^{(s)}$ to describe the configuration of the ‘‘polymers’’ instead of the real space coordinate $\mathbf{r}_i^{(s)}$ to enhance the sampling efficiency. Detailed description on the staging variables can be found elsewhere.^{30,39,42} The fictitious momentum $\mathbf{p}_i^{(s)}$ conjugate to the staging coordinate $\mathbf{u}_i^{(s)}$ and the associated fictitious mass $m_i^{\prime(s)}$ are introduced to sample the translational fluctuations. Regarding the rotational fluctuation of the molecule, we define the fictitious angular momentum $\mathbf{L}^{(s)}$ expressed in the body-fixed frame at each time slice and the related fictitious moment of inertia I'_{OCS} . Then, an effective classical Hamiltonian H_{eff} is written by

$$H_{\text{eff}} = \sum_{s=1}^M \sum_{i=1}^{N+1} \frac{(\mathbf{p}_i^{(s)})^2}{2m_i^{\prime(s)}} + \sum_{s=1}^M \frac{(\mathbf{L}^{(s)})^2}{2I'_{\text{OCS}}} + W_{\text{eff}}(\{\mathbf{U}\}, \{\Omega\}, \mathcal{P}). \quad (13)$$

Here, $\{\mathbf{U}\}$ denotes the set of all the staging coordinates over the imaginary time slices. On the basis of the effective Hamiltonian, equations of motion for $\mathbf{u}_i^{(s)}$ are derived as

$$\frac{d\mathbf{u}_i^{(s)}}{dt} = \frac{\mathbf{p}_i^{(s)}}{m_i^{\prime(s)}},$$

$$\frac{d\mathbf{p}_i^{(s)}}{dt} = -\frac{\partial W_{\text{eff}}}{\partial \mathbf{u}_i^{(s)}} = \begin{cases} -m_i \omega_0^2 (2\mathbf{u}_i^{(1)} - \mathbf{u}_{\mathcal{P}i}^{(1)} - \mathbf{u}_{\mathcal{P}^{-1}i}^{(1)}) - \frac{1}{M} \sum_{s=1}^M \partial V / \partial \mathbf{u}_i^{(1)} & (s=1) \\ -m_i^{(s)} \omega_M^2 \mathbf{u}_i^{(s)} - (1/M) \sum_{s=1}^M \partial V / \partial \mathbf{u}_i^{(s)} & (s \neq 1), \end{cases} \quad (14)$$

where \mathcal{P}^{-1} denotes an inverse permutation: $\mathcal{P}^{-1}i=j$ if $\mathcal{P}j=i$, and $V=U_{\text{He-He}}+V_{\text{He-OCS}}+V_{\text{corr}}$. Here, a characteristic frequency $\omega_0=1/\beta\hbar$ and the staging masses $m_i^{(s)}=[s/(s-1)]m_i$. The derivative of V regarding the staging variable $\partial V/\partial \mathbf{u}_i^{(s)}$ can be evaluated efficiently using $\partial V/\partial \mathbf{r}_i^{(s)}$ via a recurrence relation.^{30,39} On the other hand, quaternion parameters⁴³ are used to specify the orientation of the molecule at each time slice. The quaternion parameters at the imaginary time slice s is denoted by $\mathbf{Q}^{(s)}=(Q_0^{(s)}, Q_1^{(s)}, Q_2^{(s)}, Q_3^{(s)})$. The definition of the parameters is followed by the Goldstein convention.⁴⁴ Then, the equations of motion for rigid linear rotors can be written by⁴⁵

$$\frac{d\mathbf{Q}^{(s)}}{dt} = \frac{1}{2}\mathbf{A}[\omega^{(s)}]\mathbf{Q}^{(s)},$$

$$\frac{d\mathbf{L}^{(s)}}{dt} = \mathbf{T}^{(s)}, \quad (15)$$

where $\mathbf{T}^{(s)}$ denotes the torque on the molecule at the imaginary time slice s . The matrix $\mathbf{A}[\omega^{(s)}]$ is a 4×4 antisymmetric matrix defined by

$$\mathbf{A}[\omega^{(s)}] = \begin{pmatrix} 0 & -\omega_x^{(s)} & -\omega_y^{(s)} & -\omega_z^{(s)} \\ \omega_x^{(s)} & 0 & \omega_z^{(s)} & -\omega_y^{(s)} \\ \omega_y^{(s)} & -\omega_z^{(s)} & 0 & \omega_x^{(s)} \\ \omega_z^{(s)} & \omega_y^{(s)} & -\omega_x^{(s)} & 0 \end{pmatrix}, \quad (16)$$

where $\omega^{(s)}$ is a fictitious angular velocity in the body-fixed frame: $\omega^{(s)}=\mathbf{L}^{(s)}/I'_{\text{OCS}}$ for the rigid rotors. In the laboratory frame, the torque at a time slice s , $\mathbf{T}_L^{(s)}$, can be calculated by

$$\mathbf{T}_L^{(s)} = -\mathbf{e}^{(s)} \times \frac{\partial W_{\text{eff}}}{\partial \mathbf{e}^{(s)}} = -\mathbf{e}^{(s)} \times \frac{1}{M} \frac{\partial}{\partial \mathbf{e}^{(s)}} \{u^{\text{rot}}(\Omega^{(s-1)}, \Omega^{(s)}) + u^{\text{rot}}(\Omega^{(s)}, \Omega^{(s+1)})\} - \mathbf{e}^{(s)} \\ \times \frac{1}{M} \frac{\partial}{\partial \mathbf{e}^{(s)}} \{V_{\text{He-OCS}}(\mathbf{R}^{(s)}, \Omega^{(s)}) + V_{\text{corr}}(\mathbf{R}^{(s)}, \Omega^{(s)})\}. \quad (17)$$

Equations (14) and (15) are used to generate trial configurations in the hybrid Monte Carlo method.

The PIHMC method is summarized as follows. We start with an initial state of the system ($\{\mathbf{U}\}, \{\mathbf{Q}\}$), and resample the fictitious linear and angular momenta $\{\mathbf{P}\}$ and $\{\mathbf{L}\}$ from a Maxwell distribution. Path integral molecular dynamics is then used to move the whole system for time increment of $n_{\text{MD}} \times \Delta t$ where Δt is the time step of the MD calculation and n_{MD} is the number of MD steps in one HMC cycle. The trial configuration is accepted or rejected based on the Metropolis criterion,

$$A_{\text{HMC}} = \min[1, e^{-\beta \Delta H_{\text{eff}}}], \quad (18)$$

where A_{HMC} is the acceptance probability, and ΔH_{eff} is the change in the total energy Eq. (13) as a result of the move. We can introduce a multiple time step method to further discretize the time step Δt as $\Delta t = n_{\text{RESPA}} \times \delta t$, which can be done systematically by the reference system propagator algorithm (RESPA) method.⁴⁶ We comment on the integration method of the above equations of motion. As described

above, a time-reversible and area-preserving integrator has to be used to maintain the detailed balance condition in the HMC move. Such an integrator for rigid bodies has been developed by Matubayasi and Nakahara.⁴⁷ In the present study, we adopted their method for numerically solving Eqs. (14) and (15).

C. Permutation sampling

In the present study, we sample the permutation together with the associated path variables using the multilevel Metropolis method implemented by the bisection algorithm.¹³ To accelerate the sampling efficiency, we apply an idea of the configurational-bias Monte Carlo (CBMC)³¹ to the bisection method.

We first describe the sampling procedure briefly. The time slice at $s=1$ is chosen at random in the range $[1, M]$; we select two time slices at $s=1$ and $m+1$. Atomic coordinates at time slices outside the interval $[1, m+1]$ are kept to be fixed. For the multilevel sampling, the permutation and the successive $m-1$ time slices in the interval are partitioned into $l+1$ levels with a condition $m=2^l$. At a level $k(\geq 1)$, 2^{k-1} time slices are located in every 2^{l-k} slices in $[1, m+1]$; this corresponds to the imaginary time increment $\Delta\tau_k=2^{l-k}\Delta\tau$. The top level ($k=0$) is assigned to the permutation of the particle labels between the time slices at $s=1$ and $m+1$. Then, the permutation and the associated atomic coordinates are sampled from the top to the bottom level l . Here, we abbreviate all the variables as $x=(\bar{x}, x_0, x_1, \dots, x_l)$ where x_0 denotes the permutation \mathcal{P} , x_k the variables at a level k , and \bar{x} the fixed variables in the multilevel Metropolis move. For later use, we define a distribution function π_k describing each level as

$$\pi_k(x) \propto e^{-K_k(\bar{x}, x_0, \dots, x_k; \Delta\tau_k) - U_k(\bar{x}, x_0, \dots, x_k; \Delta\tau_k)}, \quad (19)$$

where K_k and U_k are the kinetic and interacting action at the inverse temperature $\Delta\tau_k$.⁴⁸ In the present study, the end-point approximation for the He-He correlation and the primitive approximation for the He-OCS correlation are used for U_k except the final level l where $\pi_l(x)=\pi(x)$.

At the top of the multilevel Metropolis method, the permutation is sampled between the selected time slices at $s=1$ and $m+1$. According to the heat bath method, the sampling probability is constructed using the kinetic action at the inverse temperature $\Delta\tau_0$. Then, a trial permutation is accepted based on the Metropolis criterion. When the trial permutation is accepted, we sample the associated path variables between the selected end points with the given permutation; this sampling is performed by the bisection method with the condition $\mathbf{r}_i^{(m+1)}=\mathbf{r}_{\mathcal{P}_i}^{(m+1)}$, where the primed coordinates denote the new coordinates generated by the trial moves. The bisection algorithm combined with CBMC can be described recursively. If the trial move at a level $k-1$ has been accepted, we generate n_{cb} sets of the atomic coordinates involved in the permutation at the level k by

$$\mathbf{r}'_{i,j}(s) = \frac{1}{2} \{ \mathbf{r}'_i(s-\Delta s_k) + \mathbf{r}'_i(s+\Delta s_k) \} + \eta \sqrt{\Delta \tau_k \lambda} \quad (j = 1, \dots, n_{cb}), \quad (20)$$

where $\Delta s_k = \Delta \tau_k / \Delta \tau$ and η denotes normally distributed random three vector with zero mean and unit variance. Then, we select a trial configuration out of n_{cb} configurations, which is denoted as x'_k , according to the following probability p_k^{int} :

$$p_k^{\text{int}}(x'_k) = \frac{e^{-U_k(\bar{x}, x'_0, \dots, x'_k; \Delta \tau_k)}}{W_k^{\text{int}}(n)}, \quad (21)$$

where the normalization constant $W_k^{\text{int}}(n)$ is written by

$$W_k^{\text{int}}(n) = \sum_{j=1}^{n_{cb}} e^{-U_k(\bar{x}, x'_0, \dots, x'_{k,j}; \Delta \tau_k)}. \quad (22)$$

Similarly, we generate $n_{cb}-1$ sets of the atomic coordinates for the backward move as

$$\mathbf{r}'_{i,j}(s) = \frac{1}{2} \{ \mathbf{r}'_i(s-\Delta s_k) + \mathbf{r}'_i(s+\Delta s_k) \} + \eta \sqrt{\Delta \tau_k \lambda} \quad (j = 2, \dots, n_{cb}) \quad (23)$$

and the corresponding normalization factor by

$$W_k^{\text{int}}(o) = e^{-U_k(\bar{x}, x_0, \dots, x_k; \Delta \tau_k)} + \sum_{j=2}^{n_{cb}} e^{-U_k(\bar{x}, x_0, \dots, x_{k,j}; \Delta \tau_k)}. \quad (24)$$

Then, the trial configuration at the level k is accepted by

$$A_k(x', x_k^*, x_k'^*) = \min \left[1, \frac{W_k^{\text{int}}(n)}{W_k^{\text{int}}(o)} e^{\delta U_{k-1}} \right], \quad (25)$$

where $\delta U_{k-1} = U_{k-1}(\bar{x}, x'_0, \dots, x'_{k-1}) - U_{k-1}(\bar{x}, x_0, \dots, x_{k-1})$, and the variables x'_k and $x_k'^*$ are described below. If this configuration is accepted, we go on to the next level. We continue this procedure recursively until we reach the final level. Only if the final level is accepted, the permutation and the associated path variables are updated to new one. Here, the overall acceptance is written by $A_{\text{perm}} = \prod_{k=0}^l A_k$.

We justify the above procedure. We write the set of the additional $(n_{cb}-1)$ configurations except x'_k at a level k as $x_k'^*$. Similarly, we write $(n_{cb}-1)$ configurations for the backward move at the level k as x_k^* . Then, we impose the detailed balance condition for every particular choice of the sets $x_k'^*$ and x_k^* at each level, which is referred to be the ‘‘superdetailed balance’’ condition,³¹

$$\begin{aligned} & \frac{\pi_k(x)}{\pi_{k-1}(x)} T_k(x'_k, x_k^*, x_k'^*) A_k(x', x_k^*, x_k'^*) \\ &= \frac{\pi_k(x')}{\pi_{k-1}(x')} T_k(x_k, x_k^*, x_k'^*) A_k(x, x_k^*, x_k'^*), \end{aligned} \quad (26)$$

where $T_k(x'_k, x_k^*, x_k'^*)$ is a sampling probability at the level k . The sampling probability is written by $T_k = p_k(x'_k) p_k^{\text{int}}(x_k'^*)$ where p_k is defined by

$$p_k(x'_k) \propto \frac{e^{-K_k(\bar{x}, x'_0, \dots, x'_k; \Delta \tau_k)}}{e^{-K_{k-1}(\bar{x}, x'_0, \dots, x'_{k-1}; \Delta \tau_{k-1})}}. \quad (27)$$

Equation (27) corresponds to the procedure described by Eq. (20). Acceptance probability (25) is sufficient to satisfy the superdetailed balance condition Eq. (26) at the level k . By

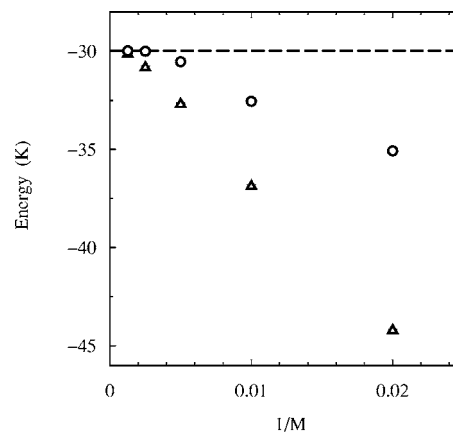


FIG. 1. Averaged total energy $\langle H \rangle$ for the He-OCS dimer at 0.37 K calculated by the primitive and Takahashi-Imada (T-I) approximations as a function of $1/M$. The OCS molecule is fixed at the origin. Open triangles are for the primitive approximation and open circles for the T-I approximation. The numerically exact result for the system is indicated by dashed line, which was reported in Ref. 55. Energies are in units of kelvin. The error bar is expressed at 95% confidence level, and is smaller than the size of the corresponding data symbol when it is not shown.

multiplying Eq. (26) over whole levels, we can verify that the total move satisfies the detailed balance condition. We can recover the standard bisection method using the kinetic action, which is called the free-particle sampling,¹³ when $n_{cb}=1$. The configurational-bias move incorporates the effect of the interatomic interaction in the free-particle sampling. Computational efficiency on the method will be presented elsewhere.⁴⁹

III. COMPUTATIONAL DETAILS

The calculated system consists of $N=64$ helium-4 atoms and a OCS molecule at the temperature 0.37 K. The number of discretization was chosen to be $M=216$ corresponding to $1/\Delta \tau=80$ K. The rotational constant of the OCS molecule was taken from a gas-phase experimental value⁵⁰ $B_{\text{OCS}}=0.20286$ cm⁻¹, which was used to construct the effective potential of quantum rotation tabulated on a fine grid. The potential of Aziz *et al.*⁵¹ was used as a pairwise interaction between two helium atoms. The morphed potential of Howson and Hutson⁵² was adopted for the He-OCS interaction. Path integral hybrid Monte Carlo calculations were performed for the system obeying Bose-Einstein statistics for both quantum and fixed OCS cases. For comparison, the system obeying Maxwell-Boltzmann statistics was also examined.

Here, we briefly examine the systematic error arising from the discretized expression of the path integral. In Fig. 1, we show the total energy of the ⁴He-OCS dimer $\langle H \rangle$ as a function of $1/M$. Temperature of the dimer was controlled to be $T=0.37$ K and the OCS molecule was fixed at the origin. Path integral calculations were performed using the standard primitive approximation^{40,41} and the Takahashi-Imada (T-I) approximation^{32,37} for $M=50, 100, 200, 400,$ and 800 . In the case of the primitive approximation, the energy is found to be slowly convergent to the numerical exact value. To obtain the accurate energy, we need the time slices more than 800. On the other hand, the energy by the T-I approximation

TABLE I. Averaged total energy $\langle H \rangle$ for the fully quantized He–OCS dimer at 0.37 K calculated by the primitive and Takahashi-Imada (T-I) approximations with $M=200$. The exact result was reported in Ref. 55 by the basis set calculations. Energies are in units of kelvin. Statistical error in the last digit at 95% confidence level is indicated in parentheses.

	Primitive	T-I	Exact
$\langle H \rangle$	-28.81(4)	-26.51(4)	-26.32

quickly converges to the exact value within the statistical error; the energy of $M=400$ reaches the exact one. Regarding the fully quantized ^4He –OCS dimer, see Table I where the averaged energies by the primitive and T-I approximations with $M=200$ are collected. The total energy is found to be remarkably improved using the T-I approximation compared with the primitive counterpart. In the calculations of the OCS(^4He)₆₄ cluster, we adopted the number of discretization $M=216$ with the T-I approximation, which gives good compromise between the computational cost and the accuracy.

IV. RESULTS

We first show the density distribution of the helium atoms around the OCS molecules $\rho(\mathbf{r})$ in Fig. 2. For a linear

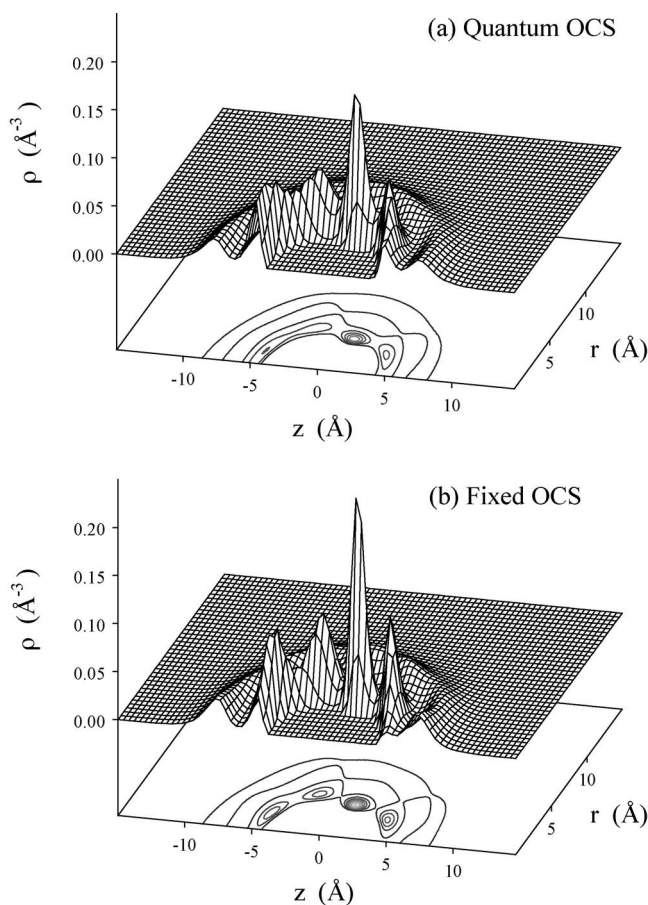


FIG. 2. The total helium density distribution around the OCS molecule $\rho(z, r)$ in the OCS(^4He)₆₄ cluster [top: $\rho(z, r)$ for the quantum OCS case; bottom: $\rho(z, r)$ for the fixed OCS case]. z is the molecular axis and r the radial distance from the z axis. The OCS center of mass is located at the origin and the molecule is oriented as O–C–S from $+z$ to $-z$. All distances are in units of angstrom.

molecule, we can write $\rho(\mathbf{r})=\rho(z, r)$ in terms of cylindrical coordinates. The density distribution in the case of the quantum dopant is presented together with the fixed dopant counterpart. In both cases, a well-developed solvation shell structure is found around the molecule. Since the density of the bulk liquid helium is $\rho=0.022 \text{ \AA}^{-3}$, much higher density region than the bulk is formed in the first solvation shell. A set of peaks seen in the first solvation shell reflects the He–OCS interaction; see Fig. 2 in Ref. 52 for details on the interaction potential. The highest peak in the solvation shell is located around the C atom where the He–OCS interaction is a minimum. We find that the rotational fluctuation of the OCS molecule gives large effects on the density distribution in the first solvation shell; the helium density in the first solvation shell is remarkably broadened by taking account of the molecular rotation. For example, the highest density around the C atom is 0.23 \AA^{-3} in the case of the fixed OCS, and the rotational fluctuation reduces the peak density to 0.16 \AA^{-3} . The effect of the quantum statistics on the density distribution is found to be much milder; the Bose statistics makes the density distribution slightly broader compared with the Boltzmann counterpart for both fixed and quantum dopant cases.

It is interesting to decompose the density distribution using the length of exchange cycles among the helium atoms, since the superfluid state of the cluster can be characterized by the long exchange cycles comparable to the system size.^{13,14} We denote the radial density profile of the helium atoms involved the exchange cycle with the length P (for $P=1, \dots, 5$) as $\rho^{(P)}(r)$. In the case of the superscript $P=6$, $\rho^{(6)}$ represents the density profile of the helium atoms involved in long exchange cycles with $P \geq 6$. The radial density profile $\rho(r)$ and the components $\rho^{(P)}(r)$, which are measured from the OCS center of mass, are presented in Fig. 3. A subpeak at $r=3.7 \text{ \AA}$ in the primary peak of the total density profile comes from the highest peak density around the C atom seen in Fig. 2. As previously found in PIMC calculations of the fixed OCS in the helium clusters,^{3,16} the total density profile is composed of two major components: one is $\rho^{(1)}$ and the other is $\rho^{(6)}$. Other components from short exchange cycles $P=2, \dots, 5$ add only small contributions to the total density profile. According to Kwon *et al.*,^{3,16} we may regard $\sum_{P=1}^5 \rho^{(P)}(r)$ as a local disturbance of the superfluidity, and $\rho^{(6)}(r)$ as a superfluid component. As seen in the figure, dominant contribution of the nonsuperfluid component is found in the first solvation shell; highest peak is located at the substructure of the total density profile where the OCS–helium interaction is a minimum. The rotational fluctuation of the molecule remarkably reduces the peak density of $\rho^{(1)}$, and on the other hand, augments the $\rho^{(6)}$ component in the first solvation shell. Here, we define the first solvation shell using the minimum of $\rho(r)$ at $r=5.9 \text{ \AA}$. The coordination number in the first solvation shell was calculated to be 21 for both quantum and fixed OCS cases. In the first solvation shell for the fixed OCS case, the superfluid component $\rho^{(6)}$ occupies 74% in the total density, and the rotational motion enhances the occupancy to 81% due to the above structural changes in the density distributions. Note that the above superfluid component does not exactly correspond to the super-

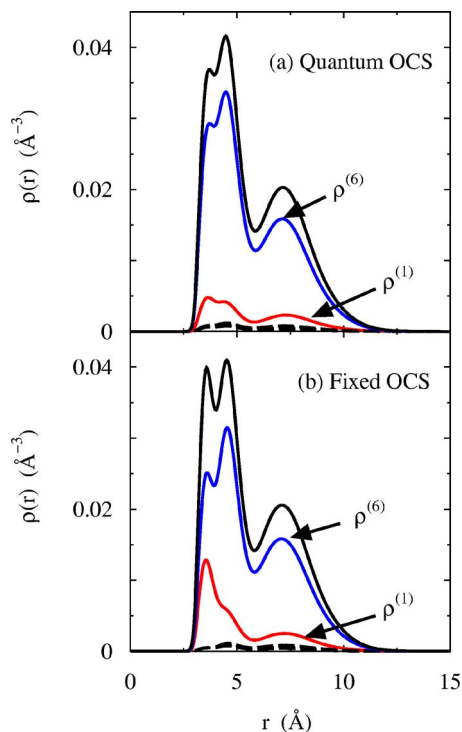


FIG. 3. (Color online) The radial density profiles of the helium atoms measured from the OCS center of mass are shown for the quantum OCS (upper panel) and the fixed OCS (lower panel). Total density profile $\rho(r)$ (black solid line), $\rho^{(1)}(r)$ (red solid line), $\rho^{(P)}(r)$ for $P=2, \dots, 5$ (black dashed lines), and $\rho^{(6)}(r)$ (blue solid line) are presented. All distances are in units of angstrom.

fluid response to an imposed rotation, although $\rho^{(6)}(r)$ qualitatively captures the superfluidity around the molecule. Draeger and Ceperley¹⁸ have developed an estimator of the local superfluid response where each cycle's contribution is properly weighted so as to recover the total superfluid response about a given rotation axis.

The energies of the doped clusters are collected in Table II. As seen in the density profiles, the solvation structure around the molecule is remarkably broadened in the first solvation shell by including the rotational fluctuation of the dopant. This results in the smaller He–OCS and He–He interaction energies compared with the fixed dopant energies. The translational kinetic energy decreases with including the molecular rotational fluctuation. This is also ascribed to the density decrement of the first solvation shell. The resulting total energy in the case of the quantum dopant is found to be smaller than that of the fixed dopant case. It is worthwhile to note that the rotational kinetic energy is 9.68 K, which is much larger than the corresponding classical value 0.37 K.

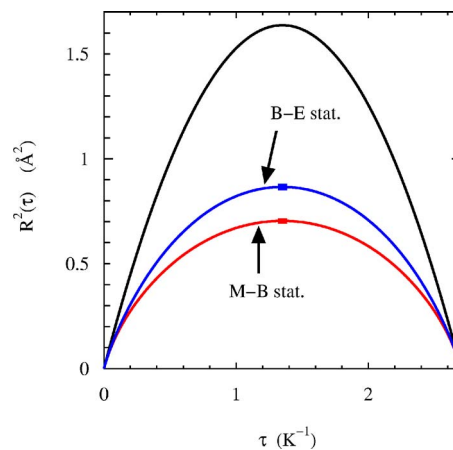


FIG. 4. (Color online) The mean square correlation function of the OCS center of mass in the imaginary time, $R^2(\tau)$ for the Bose cluster (blue solid line), and the Boltzmann cluster (red solid line). The $R^2(\tau)$ function for the free OCS molecule (black solid line) is also presented. The error bar of $R^2(\beta/2)$ is expressed at 95% confidence level.

Similarly, the increase from the classical value is also observed for the translational kinetic energy of the OCS molecule.

Next, we present the results on imaginary time fluctuations of the OCS molecule. We first show translational motion of the center of mass of the OCS molecule. The translational correlation is well described by the following mean square correlation function:

$$R^2(\tau) = \langle |\mathbf{r}_{N+1}(\tau) - \mathbf{r}_{N+1}(0)|^2 \rangle, \quad (28)$$

where $\mathbf{r}_{N+1}(\tau)$ denotes the center of mass position of the OCS molecule at an imaginary time τ . This correlation function is periodic in $[0, \beta]$. The correlation function at $\tau = \beta/2$ reflects the quantum delocalization of the center of mass of the molecule. For a free OCS molecule, the correlation function can be expressed analytically,⁵³

$$R^2(\tau) = \frac{3\beta\hbar^2}{m_{\text{OCS}}} \left[\frac{\tau}{\beta} \left(1 - \frac{\tau}{\beta} \right) \right], \quad (29)$$

where m_{OCS} denotes the total mass of the OCS molecule. The calculated results are presented in Fig. 4. Since the molecule interacts with the surrounding helium atoms, the translational fluctuation is suppressed compared with the free OCS molecule for both clusters. This causes the translational kinetic energy increase of the OCS molecule from the classical value (see Table II). It is found that the $R^2(\beta/2)$ for the Bose cluster is larger than that for the Boltzmann cluster: $R^2(\beta/2) = 0.87 \text{ \AA}^2$ for the Bose cluster and 0.70 \AA^2 for the

TABLE II. The translational kinetic energy ($\langle T^{\text{tra}} \rangle$), the rotational kinetic energy ($\langle T^{\text{rot}} \rangle$), the He–OCS, and He–He interaction energies ($\langle V_{\text{He–OCS}} \rangle$ and $\langle V_{\text{He–He}} \rangle$), and the total energy ($\langle H \rangle$) for the OCS(⁴He)₆₄ cluster obeying the Bose-Einstein statistics. The translational kinetic energy of the OCS molecule ($\langle T^{\text{tra}}_{\text{OCS}} \rangle$) is also shown. The energies are presented for the quantum and fixed OCS cases and are in units of kelvin. Statistical error in the last digit at 95% confidence level is indicated in parentheses.

	$\langle T^{\text{tra}} \rangle$	$\langle T^{\text{rot}} \rangle$	$\langle V_{\text{He–OCS}} \rangle$	$\langle V_{\text{He–He}} \rangle$	$\langle H \rangle$	$\langle T^{\text{tra}}_{\text{OCS}} \rangle$
Quantum OCS	791(1)	9.68(6)	–587.5(2)	–807.0(4)	–593.9(9)	9.7(1)
Fixed OCS	813.4(6)	...	–615.0(2)	–818.8(2)	–620.4(5)	...

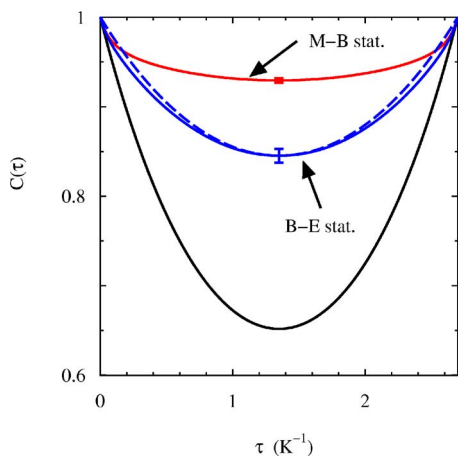


FIG. 5. (Color online) The orientational correlation function $C(\tau)$ of the OCS molecule for the Bose cluster (blue solid line) and the Boltzmann cluster (red solid line) as a function of the imaginary time τ . The size of the cluster N is 64 for both cases. The free-rotor correlation function with a gas-phase experimental B_{OCS} (black solid line) and that with a B_{eff} estimated by the $C(\beta/2)$ value of the $\text{OCS}({}^4\text{He})_{64}$ Bose cluster (blue dashed line) are also shown. The error bar about $C(\beta/2)$ is expressed at 95% confidence level.

Boltzmann cluster. This indicates that the effect of the spatial confinement of the OCS molecule by the surrounding solvent atoms is weaker in the case of the Bose cluster than the Boltzmann counterpart. This is due to the slightly broader density distribution of the helium atoms around the molecule when the Bose statistics is taken into account.

Finally, we examine the rotational motion of the OCS molecule.⁵⁴ The rotational fluctuation can be probed by the following orientational correlation function:

$$C(\tau) = \langle \mathbf{e}(\tau) \cdot \mathbf{e}(0) \rangle, \quad (30)$$

where $\mathbf{e}(\tau)$ is a unit vector proportional to the molecular axis at an imaginary time τ . This correlation function is again periodic in the imaginary time interval $[0, \beta]$. Calculated correlation functions are presented in Fig. 5 for the Bose and Boltzmann clusters. The correlation function for an isolated OCS using the gas-phase experimental $B_{\text{OCS}} = 0.20286 \text{ cm}^{-1}$ is also presented; here, we used the following analytical expression of $C(\tau)$ for a free linear rotor with a rotational constant B :⁵⁵

$$C(\tau) = \frac{1}{Z} \left\{ e^{-2B\tau} + \sum_{J>0} e^{-\beta BJ(J+1)} [J e^{B2J\tau} + (J+1) e^{-B2(J+1)\tau}] \right\}, \quad (31)$$

with $Z = \sum_{J=0}^{\infty} (2J+1) e^{-\beta BJ(J+1)}$. Suppression of the orientational fluctuation is found due to the He–OCS interaction in both Bose and Boltzmann clusters compared with the gas-phase OCS. However, the orientational fluctuation is much enhanced in the Bose cluster compared with the Boltzmann counterpart, indicating the large impact of the Bosonic correlation among the helium atoms on the rotational motion of the molecule. Using the correlation function for the Bose cluster, we estimated an effective rotational constant B_{eff} of the solvated OCS in such a way that the value of $C(\beta/2)$ was fitted to the free-rotor expression Eq. (31) at $\tau = \beta/2$; in this procedure, B was treated as a fitting parameter. The resulting

value was found to be $B_{\text{eff}} = 0.084 \pm 0.004 \text{ cm}^{-1}$, which is in reasonable agreement with the experimental value of the nanodroplet $B_{\text{eff}} = 0.0732 \text{ cm}^{-1}$.⁵⁶ An effective moment of inertia I_{eff} defined by $B_{\text{eff}} \equiv \hbar^2/2I_{\text{eff}}$ was estimated to be $201 \pm 11 \text{ amu } \text{\AA}^2$, which is comparable with the experimental value for the nanodroplet, $I_{\text{eff}} = 230 \text{ amu } \text{\AA}^2$.⁵⁶ The small (but non-negligible) discrepancy between the present calculation and the experimental nanodroplet value will be discussed in the companion paper II.¹² In Fig. 4, we show a free-rotor correlation function using the estimated B_{eff} . We find the $C(\tau)$ for the solvated OCS in the Bose cluster is well described by the free-rotor $C(\tau)$ with the B_{eff} . This demonstrates that our method realizes the effective free rotation of the OCS molecule in the superfluid cluster.

V. DISCUSSION

In this paper, we have presented the path integral hybrid Monte Carlo method for rotating molecules in quantum fluids. A novel method to handle the molecular rotation in the hybrid Monte Carlo was developed by introducing the effective potential of quantum rotation. To account for the Bose symmetry of the particles, we adopted the multilevel Metropolis method combined with the configurational-bias Monte Carlo technique. The method was successfully applied to the $\text{OCS}({}^4\text{He})_{64}$ cluster in a superfluid state. Systematic analysis on the molecular rotational fluctuation of the $\text{OCS}({}^4\text{He})_N$ is presented in the companion paper II.¹² In the following, we discuss the techniques developed in the present study.

A. Molecular dynamics and hybrid Monte Carlo methods for rigid bodies

Path integral molecular dynamics and hybrid Monte Carlo methods have been well established to sample the translational fluctuation in quantum many-body systems where the indistinguishability of the particles (the Bose-Einstein or the Fermi-Dirac statistics) is irrelevant.^{30,57} The translational density matrix directly leads the harmonic interaction in the classical system introduced by the path integral method. Various efficient sampling techniques were developed based on a variable transformation (partially) diagonalizing the harmonic interaction such as staging or normal mode variable.^{30,57} On the other hand, the rotational density matrix cannot be simplified analytically as in the translational density matrix [see, for example Eq. (6)]. Although path integral Monte Carlo methods have been devised for treating rigid rotors,³² molecular dynamics techniques are not well matured. To our knowledge, Del Buono *et al.*⁵⁸ have developed a path integral molecular dynamics method for rigid bodies, which was applied to the liquid water at room temperature. Their method is based on a semiclassical approximation of the rotational density matrix. In the present study, the effective potential of quantum rotation is introduced using the exact rotational density matrix which is converged about the quantum number J and is positive.⁵⁹ This technique is readily applicable to the molecular dynamics and hybrid Monte Carlo methods. While the effective potential method was applied to the linear rotor in the present

study, we can extend the method to other types of rigid bodies such as spherical, symmetric, and asymmetric tops. The rotational density matrix for the tops at an inverse temperature $\Delta\tau$ can be written by $\rho^{\text{rot}}(\omega, \omega'; \Delta\tau)$ where ω denotes the Euler angles relating the body-fixed frame with the laboratory frame.³² As in the linear rotors, the effective potential of quantum rotation can be introduced by $u^{\text{rot}}(\omega, \omega') \equiv -\ln \rho^{\text{rot}}(\omega, \omega') / \Delta\tau$. Even though $\rho^{\text{rot}}(\omega, \omega'; \Delta\tau)$ cannot be accessible analytically, it can be computed numerically to very high precision. This technique is useful to construct the path integral molecular dynamics and hybrid Monte Carlo algorithms for the rigid bodies. The equations of motion by the quaternion parameters can readily be used for the hybrid Monte Carlo for rigid bodies. Regarding the molecular dynamics, a massively thermostating technique^{30,57} may be useful for the efficient sampling; however, we need more experiences on this point.

B. Multilevel Metropolis method with a configurational-bias technique

We have adopted the multilevel Metropolis method¹³ where the permutation is sampled together with the associated path variables. In our previous study on the path integral hybrid Monte Carlo for correlated Bose fluids,³⁹ we used the free-particle kinetic action to generate the path variables for a given permutation. Since several particles are simultaneously involved in the permutation change, correlation among the particles must be taken into account in generating the trial position of the particles for the efficient sampling. In PIMC calculations for the superfluid helium, correlated sampling^{13,60} introducing a force bias in the trial moves has been employed to generate the trial positions. Including the effect of atomic interaction in the transition probability is important to make acceptance ratio higher. As an alternative to the above correlated sampling method, we have devised the configurational-bias move³¹ applied to the multilevel Metropolis method in the present study. At each level, a set of trial positions is generated by the free-particle kinetic action. One trial position is selected by a probability proportional to the external Boltzmann factor calculated by the interacting part of the action. Then, the trial position is accepted based on a Metropolis criterion satisfying the “superdetailed balance” condition.³¹ In this method, an energetically favorable position is preferentially selected; overlapping particle positions are efficiently excluded. This method is easily implemented in an existing bisection code, while the correlated sampling by Ceperley needs a sampling potential which has to be numerically calculated prior to path integral simulations.

ACKNOWLEDGMENTS

The author thanks Research Center for Computational Science, National Institutes of Natural Sciences for the use of supercomputers. This work was supported by the Next Generation Super Computing Project, Nanoscience Program, MEXT, Japan.

- ¹J. P. Toennies and D. F. Vilesov, *Annu. Rev. Phys. Chem.* **49**, 1 (1998), and references therein.
- ²J. P. Toennies and D. F. Vilesov, *Angew. Chem., Int. Ed.* **43**, 2622 (2004), and references therein.
- ³Y. Kwon, P. Huang, M. V. Patel, D. Blume, and K. B. Whaley, *J. Chem. Phys.* **113**, 6469 (2000), and references therein.
- ⁴M. Barranco, R. Guardiola, S. Hernández, R. Mayol, J. Navarro, and M. Pi, *J. Low Temp. Phys.* **142**, 1 (2006), and references therein.
- ⁵S. Grebenev, J. P. Toennies, and A. F. Vilesov, *Science* **279**, 2083 (1998).
- ⁶J. Tang, Y. Xu, A. R. W. McKellar, and W. Jäger, *Science* **297**, 2030 (2002).
- ⁷Y. Xu, W. Jäger, J. Tang, and A. R. W. McKellar, *Phys. Rev. Lett.* **91**, 163401 (2003).
- ⁸J. Tang, A. R. W. McKellar, F. Mezzacapo, and S. Moroni, *Phys. Rev. Lett.* **92**, 145503 (2004).
- ⁹Y. Xu, N. Blinov, W. Jäger, and P.-N. Roy, *J. Chem. Phys.* **124**, 081101 (2006).
- ¹⁰W. Topic, W. Jäger, N. Blinov, P.-N. Roy, M. Botti, and S. Moroni, *J. Chem. Phys.* **125**, 144310 (2006).
- ¹¹A. R. W. McKellar, Y. Xu, and W. Jäger, *Phys. Rev. Lett.* **97**, 183401 (2006).
- ¹²S. Miura, *J. Chem. Phys.* **126**, 114309 (2007).
- ¹³D. M. Ceperley, *Rev. Mod. Phys.* **67**, 279 (1995), and references therein.
- ¹⁴P. Sindzingre, M. L. Klein, and D. M. Ceperley, *Phys. Rev. Lett.* **63**, 1601 (1989).
- ¹⁵Y. Kwon, D. M. Ceperley, and K. B. Whaley, *J. Chem. Phys.* **104**, 2341 (1996).
- ¹⁶Y. Kwon and K. B. Whaley, *Phys. Rev. Lett.* **83**, 4108 (1999).
- ¹⁷Y. Kwon and K. B. Whaley, *J. Chem. Phys.* **115**, 10146 (2001).
- ¹⁸E. W. Draeger and D. M. Ceperley, *Phys. Rev. Lett.* **90**, 065301 (2003).
- ¹⁹M. V. Patel, A. Vies, F. Paesani, P. Huang, and K. B. Whaley, *J. Chem. Phys.* **118**, 5011 (2003).
- ²⁰F. Paesani, A. Viel, F. A. Gianturco, and K. B. Whaley, *Phys. Rev. Lett.* **90**, 073401 (2003).
- ²¹S. Moroni, A. Sarsa, S. Fantoni, K. E. Schmidt, and S. Baroni, *Phys. Rev. Lett.* **90**, 143401 (2003).
- ²²S. Moroni, N. Brinov, and P.-N. Roy, *J. Chem. Phys.* **121**, 3577 (2004).
- ²³F. Paesani and K. B. Whaley, *J. Chem. Phys.* **121**, 4180 (2004).
- ²⁴S. Paolini, S. Fantoni, S. Moroni, and S. Baroni, *J. Chem. Phys.* **123**, 114306 (2005).
- ²⁵S. Miura, *J. Phys.: Condens. Matter* **17**, S3259 (2005).
- ²⁶R. E. Zillich, F. Paesani, Y. Kwon, and K. B. Whaley, *J. Chem. Phys.* **123**, 114301 (2005).
- ²⁷N. Blinov and P.-N. Roy, *J. Low Temp. Phys.* **140**, 253 (2005).
- ²⁸S. Duane, A. D. Kennedy, B. J. Pendleton, and D. Roweth, *Phys. Lett. B* **195**, 216 (1987).
- ²⁹B. Mehlig, D. W. Heermann, and B. M. Forrest, *Phys. Rev. B* **45**, 679 (1992).
- ³⁰M. Tuckerman, B. J. Berne, G. J. Martyna, and M. L. Klein, *J. Chem. Phys.* **99**, 2796 (1993).
- ³¹D. Frenkel and B. Smit, *Understanding Molecular Simulation: From Algorithms to Applications*, 2nd ed. (Academic, New York, 2002).
- ³²D. Marx and M. H. Müser, *J. Phys.: Condens. Matter* **11**, R117 (1999), and references therein.
- ³³R. P. Feynman and A. R. Hibbs, *Quantum Mechanics and Path Integrals* (McGraw-Hill, New York, 1965).
- ³⁴R. P. Feynman, *Statistical Mechanics* (Addison-Wesley, Redwood City, 1972).
- ³⁵M. H. Müser, *Mol. Simul.* **17**, 131 (1996).
- ³⁶C. Chakravarty, M. C. Gordillo, and D. M. Ceperley, *J. Chem. Phys.* **109**, 2123 (1998).
- ³⁷M. Takahashi and M. Imada, *J. Phys. Soc. Jpn.* **53**, 3765 (1984).
- ³⁸S. Miura and S. Okazaki, *J. Chem. Phys.* **115**, 5353 (2001).
- ³⁹S. Miura and J. Tanaka, *J. Chem. Phys.* **120**, 2160 (2004).
- ⁴⁰D. Chandler and P. G. Wolynes, *J. Chem. Phys.* **74**, 4078 (1981).
- ⁴¹D. Chandler, in *Liquids, Freezing, and Glass Transition*, edited by J. P. Hansen, D. Levesque, and J. Zinn-Justin (Elsevier, Amsterdam, 1991).
- ⁴²E. L. Pollock and D. M. Ceperley, *Phys. Rev. B* **30**, 2555 (1984).
- ⁴³M. P. Allen and D. J. Tildesley, *Computer Simulations of Liquids* (Clarendon, Oxford, 1987).
- ⁴⁴H. Goldstein, *Classical Mechanics* (Addison-Wesley, Reading, 1980).
- ⁴⁵For nonlinear molecules, the second equation becomes $\dot{\mathbf{L}}^{(s)} + \omega^{(s)} \times \mathbf{L}^{(s)} = \mathbf{N}^{(s)}$.
- ⁴⁶M. Tuckerman, G. J. Martyna, and B. J. Berne, *J. Chem. Phys.* **97**, 1990

(1992).

⁴⁷N. Matubayasi and M. Nakahara, J. Chem. Phys. **110**, 3291 (1999).

⁴⁸Here, the kinetic and interacting actions have no dimension. For example, the interacting part of the action at the bottom level l is defined using $\Delta\tau\{U_{\text{He-He}}+V_{\text{He-OCS}}+V_{\text{corr}}\}$.

⁴⁹S. Miura (unpublished).

⁵⁰N. Hunt, S. C. Foster, J. W. C. Johns, and A. R. W. McKellar, J. Mol. Spectrosc. **111**, 42 (1985).

⁵¹R. A. Aziz, A. R. Janzen, and M. Moldover, Phys. Rev. Lett. **74**, 1586 (1995).

⁵²J. M. M. Howson and J. M. Hutson, J. Chem. Phys. **115**, 5059 (2001).

⁵³A. L. Nichols III, D. Chandler, Y. Singh, and D. M. Richardson, J. Chem. Phys. **81**, 5109 (1984).

⁵⁴Preliminary calculations on the orientational correlation function of the OCS molecule doped in Bose and Boltzmann clusters are presented in

Ref. [25](#). Similar calculations on the CO₂ doped helium clusters can be found in Ref. [27](#).

⁵⁵N. Blinov, X. G. Song, and P.-N. Roy, J. Chem. Phys. **120**, 5916 (2004).

⁵⁶S. Grebenev, M. Hartmann, M. Havenith, B. Sartakov, J. P. Toennies, and A. F. Vilesov, J. Chem. Phys. **112**, 4485 (2000).

⁵⁷M. E. Tuckerman and A. Hughes, in *Classical and Quantum Dynamics in Condensed Phase Simulations*, edited by B. J. Berne, G. Ciccotti, and D. F. Coker (World Scientific, Singapore, 1999).

⁵⁸G. S. Del Buono, P. J. Rossky, and J. Schnitker, J. Chem. Phys. **95**, 3728 (1991).

⁵⁹When the indistinguishability of the nuclei involved in the rotation of a molecule is relevant, there is a possibility that the rotational density matrix has a negative value. See Ref. [32](#) for detailed discussion.

⁶⁰D. M. Ceperley and E. L. Pollock, Phys. Rev. Lett. **56**, 351 (1986).